NRIAG Journal of Astronomy and Geophysics 7 (2018) 297–308

Contents lists available at ScienceDirect

NRIAG Journal of Astronomy and Geophysics

journal homepage: www.elsevier.com/locate/nrjag

Full length article

Integration of airborne geophysical and satellite imagery data to delineate the radioactive zones at west Safaga Area, Eastern Desert, Egypt

Salem Barbary Ahmed

Nuclear Materials Authority, P.O. Box 530, El Maadi, Cairo, Egypt

ARTICLE INFO

Keywords:
Radioactive zones
Spectrometric
Aeromagnetic
Central eastern desert

ABSTRACT

The main topic of this study is to use the airborne geophysical data and the satellite images to reveal the structural setting that affect in the distribution of the radioactive minerals in west Safaga Area. The gamma-ray spectrometric maps are useful to delineate the boundaries of the rock units. The radioelement maps of K%, eU and eTh provide, on a single display, an overall picture of the radioelement distributions across the study area. The high radiometric anomalies are concentrated over the granitic rocks and the granite dykes at the south-eastern and northwestern parts of the study area.

The magnetic data reduced to the north magnetic pole (RTP) was separated to regional and residual magnetic component maps to reveal the major deep structures in the area. The depth estimation of shallow and deep seated interfaces were calculated through the application of power spectral analysis of the aeromagnetic data, two main average interfaces at depths 0.2 and 0.56 Km below the measuring level.

From the interpretation of false colored composite images of Landsat-5(TM) and ASTER, (bands 2, 4 & 7 for Landsat-5(TM) and bands 7, 3, 1 for ASTER) in RGB, it is easy to distinguish the boundaries between rock units, according to color differences and photo geological characteristics of the rocks, in addition to the band ratio of, 5/7, 5/1, 5/4 for Landsat TM and the band ratio of 4/7, 4/1, 4/3 for ASTER) in RGB, respectively.

Integration of the gamma-ray spectrometric, magnetic maps and the processed satellite images(Landsat-5(TM) and ASTER images), revealed approximately rapprochement between the high radiation zones, brakes between the high and low magnetic amplitude and the surface observed faults and the fractures in the locations between the rock types boundaries in the studied area.

1. Introduction

The study area is located in the Central Eastern Desert of Egypt, between latitudes 26°38′ and 26°50′N and longitudes 33°32′ and 33°56′E. It covers a surface area of about 600 km^2 (Fig. 1). The previous works of the study area showed that the area including some structures, which are associated by the collections of some minerals accompanied the radioactive minerals. Generally, the youngest, felsic and potassic igneous rocks are rich in radioactive minerals such as uranium and thorium (Rogers and Adams, 1969). Most of radioactive occurrences in the basement rocks of Egypt are in the granites and associated peigmatites. The high radioactivity level of these rocks is related to the presence of other minerals e.g. zircon, monazite, thorite, uranothorite and allanite (Schürmann, 1966). There are few detailed investigations combined with radiometric and mineralogical studies were conducted on the study area (El Hadary et al., 2013). The analysis of airborne spectrometric, magnetic data, and satellites imagery was performed for delineating the locations of the structural lineaments which affected in the distribution of the radioelements in the study area. The spectrometric maps of the study area will help to locate the high alteration areas of the radioactive minerals, and discriminate the boundaries of the different rocks. From the aeromagnetic maps, it will be easy to reveal the structural pattern which will be associated to the minerals collections. From the interpretation of the satellite images of the study area, it can detect the places of the surface structural features (contact fractures, faults and shear zones).

1.2. Geologic setting

The study area is covered with Precambrian basement rocks that comprise older granitoids, younger granites and Dokhan Volcanic which injected by basic and acidic dykes of different trends (Fig. 2). The exposed rock units are traversed by several wadis (valleys) filled with alluvial deposits of Quaternary age.

Peer review under responsibility of National Research Institute of Astronomy and Geophysics.
E-mail address: salemgeo@yahoo.com.

https://doi.org/10.1016/j.nrjag.2018.07.005
Received 13 March 2018; Received in revised form 25 April 2018; Accepted 21 July 2018
Available online 31 July 2018

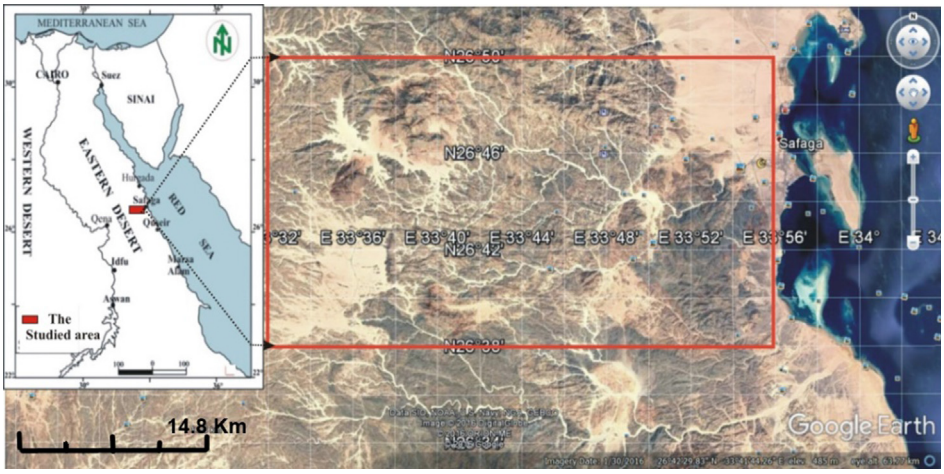

Fig. 1. The location map of the study Area.

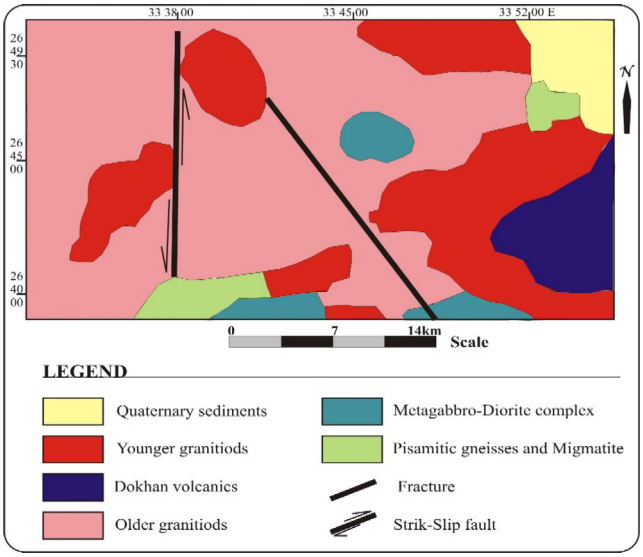

Fig. 2. Geological map of the West Safaga Area, (after Conoco & EGPC, 1987), colors modified.

The different main rock units in the study area are chronologically arranged from top to bottom as illustrated from the geologic map (Conoco & EGPC, 1987) as the following sequences (Fig. 2):

(4) Post granitic dykes ..... (Youngest)

(3) Younger granites (GII & GIII granites)

(2) Dokhan volcanics { (Acidic) / (Intermediate)

(1) Older granitoids (GI granites) ..... (Oldest)

The older granitoids range in composition from granodiorite to quartz diorite through tonalite. However, the younger granites range in composition from syenogranites to alkali feldspar granites. The different types of the Dokhan volcanics constitute a definite and well-marked association corresponding to the well-known basalt-andesite-rhyolite association.

The basic dykes are the youngest and the prevalent ones. They are widespread and concentrated in different parts of the study area and are basaltic in composition. The basic dykes are noticed intersect acidic ones (rhyolites and micro granite).

The acidic dykes are less in number and have large size and space compared to basic ones. They form high and huge blocks with irregular shapes. The microgranite dykes occur as swarms of abnormal radioactivity and poly mineralization.

Most occurrence of radioactive minerals of Egypt are in granites and associated pegmatites. Several Nb-Ta occurrences have been recorded in different localities of the Eastern desert (Raslan & Ali, 2011).

2. Data used

The geological map, satellite images and airborne gamma-ray spectrometric and magnetic data have been used to determine the structural lineaments crossing the area, and also to delineate the radiometric anomalous areas in the study area. The airborne data used in the study area were produced in 1984 by Aero Service Division of Western Geophysical Company of America. The surveying was carried out through parallel flight lines oriented in the NE-SW direction at 1.5 Km spacing. Meanwhile, the tie lines were in the northwestern-south eastern direction with 10 Km intervals (Aero-service, 1984).

The airborne geophysical data are represented by the total-count radiometric (Tc in Ur), potassium (K in %), equivalent uranium (eU in ppm) and equivalent thorium (eTh in ppm), also the total magnetic field intensity measurements reduced to the north pole (RTP in nT). Processing of these data has been carried out using Oasis Montage Data Processing and Analyses (Geosoft, 2002).

Resampling was carried out to project the produced data from ETM (Egyptian Traverse Mercator – Red Belt) system to UTM (Universal Traverse Mercator) system. This process was necessary to achieve compatibility with satellites images to ensure the coincidence between the different layers that could be extracted from both types of data.

2.1. Airborne gamma-ray spectrometric data

The surveying of airborne spectral radiometric of the study area provided valuable information for four parameters (variables) namely: total-count of the gamma radiation (TC, in Ur), absolute occurrence of the three radioelements: potassium (K^{40}, in %), equivalent uranium (eU, in ppm) and equivalent thorium (eTh, in ppm).

The surface concentrations of the radioelements: potassium, uranium and thorium, can be determined by measurements of intensities of gamma-ray radiation emitted. These data are then used to compile maps showing the three radioelements and their ratios. From mineral exploration and metallogenic points of view, ratios have more significance than absolute abundances.

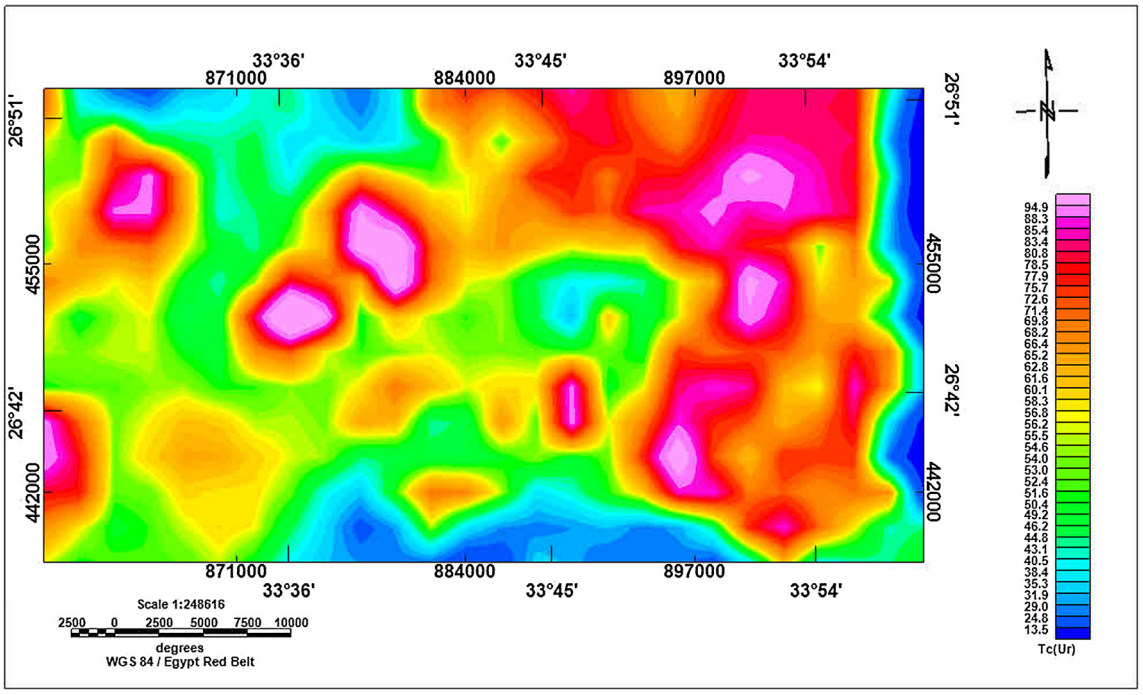

Fig. 3. Total-count (TC) radiometric map (in Ur) of west Safaga area.

2.2. Airborne spectrometric data interpretation

The four parameters namely: (TC, in Ur), (K, in %), (eU, in ppm) and (eTh, in ppm) (Figs. 3–6) show relative variation of the gamma radiation. The occurrence of three radioelements reflects the lateral variation of surface elemental concentration of different rock and soil types. The major trend from the four radiometric maps is the NW-SE trend.

The four spectrometric maps are classified depending on the distribution that include three levels as follow:

1. The lowest level (from bright blue to green) is encountered in the four radiometric maps, it is conjugated with the part of the area covering the metagabbro and the wadi deposits and it have the same feature of no radiometric effect.
2. The intermediate level (from green to yellow) is founded over the area of valleys filled with alluvial deposits of Quaternary age. This level is clearly shown in the four radioactive maps.
3. The highest level (from yellow to magenta) is associated with younger granites, older granites, Dokhan Volcanics and the microgranite dykes

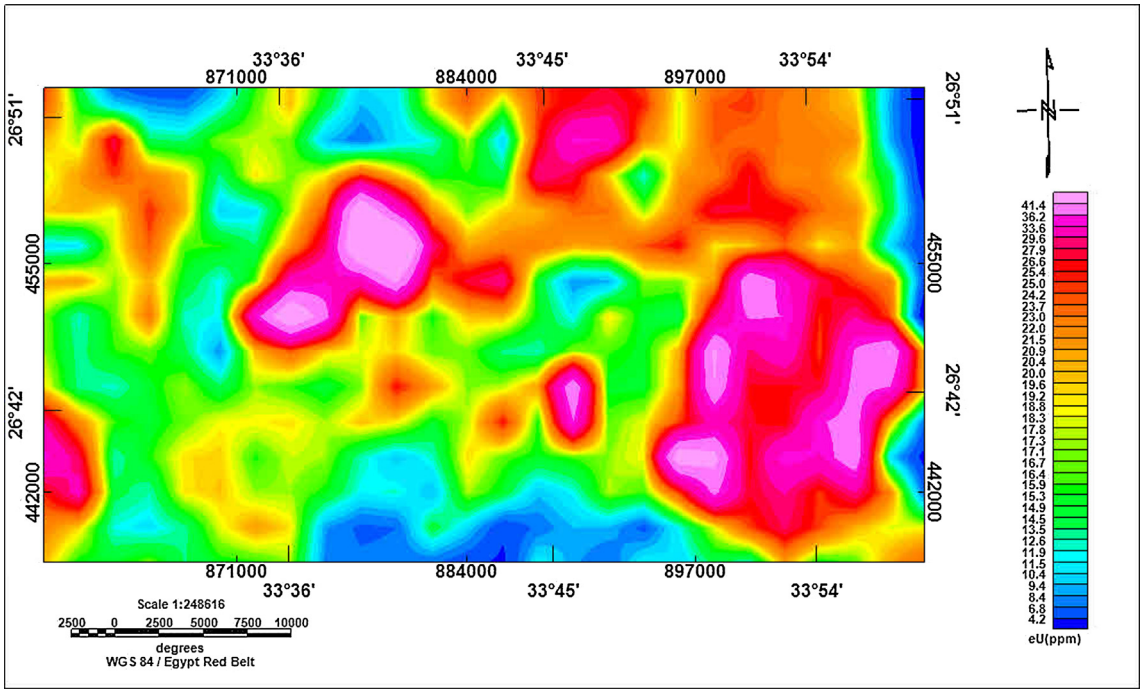

Fig. 4. Equivalent uranium (eU) map (in ppm) of West Safaga area.

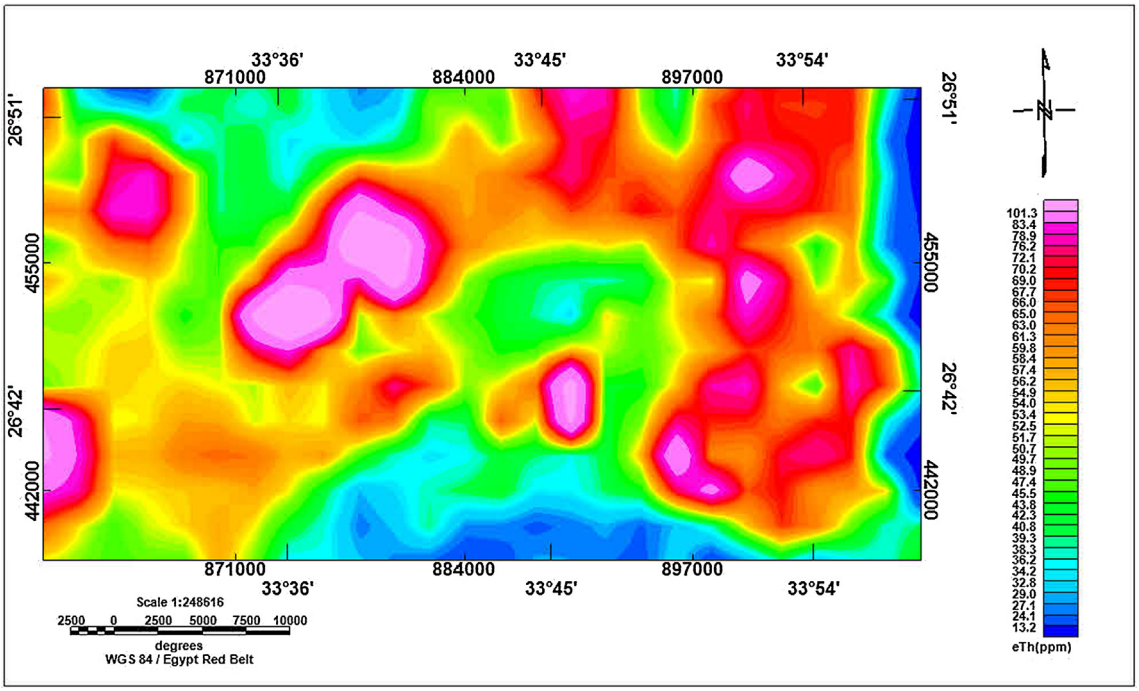

Fig. 5. Equivalent thorium (eTh) map (in ppm) of West Safaga area.

2.3. Ternary radioelement maps

A ternary radioelement map is a color composite image generated by modulating the red, blue and green phosphors of the display device or yellow, cyan and magenta dyes of a printer in proportions to the radioelement concentration values of K%, eU and eTh grids. The applying of red, green and blue for K%, eU, and eTh respectively, displaying gamma-ray spectrometric data (IAEA, 2003).

The three radioelements composite image maps of the study area are generated from the gamma-ray spectrometric data K%, eU and eTh show the variation occurring in the three radioelement concentration which mainly reflect lithological variations. The color of the triangular legend is (Potassium in red, Equivalent Thorium in blue and Equivalent Uranium in green) indicates 100% concentration of the indicated radioelement. The color inside the triangle represents different ratio of the radioelement according to the color differences on the absolute three radioelement composite image maps.

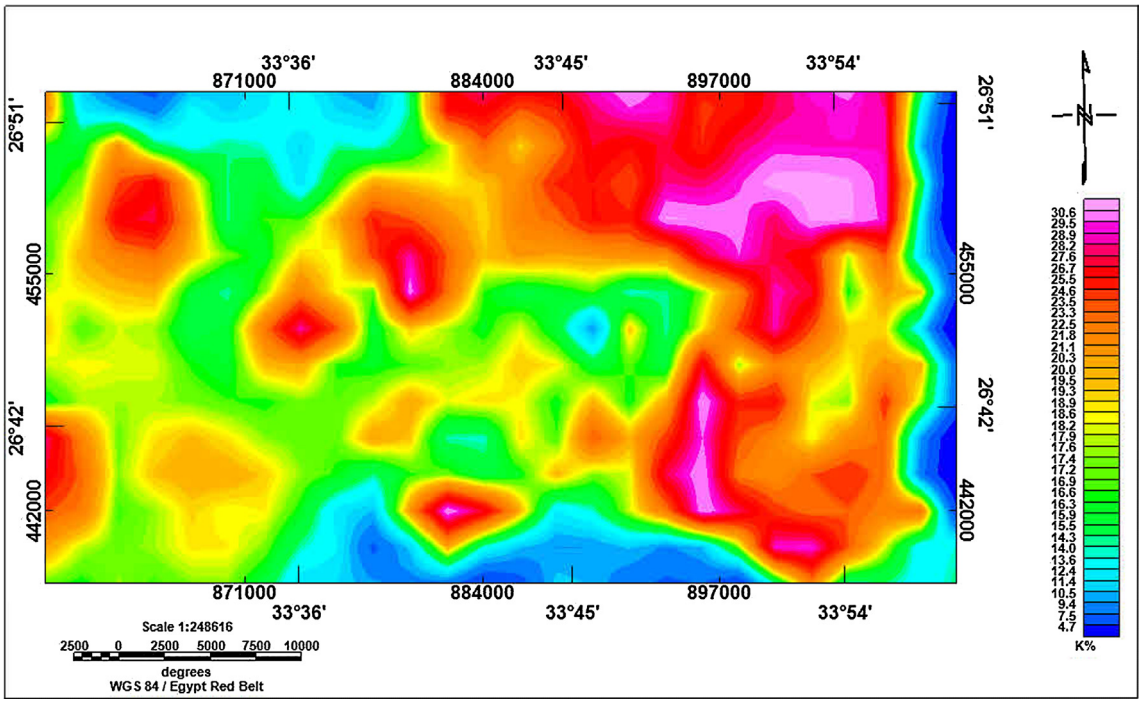

Fig. 6. Potassium (K) map (in %) of West Safaga area.

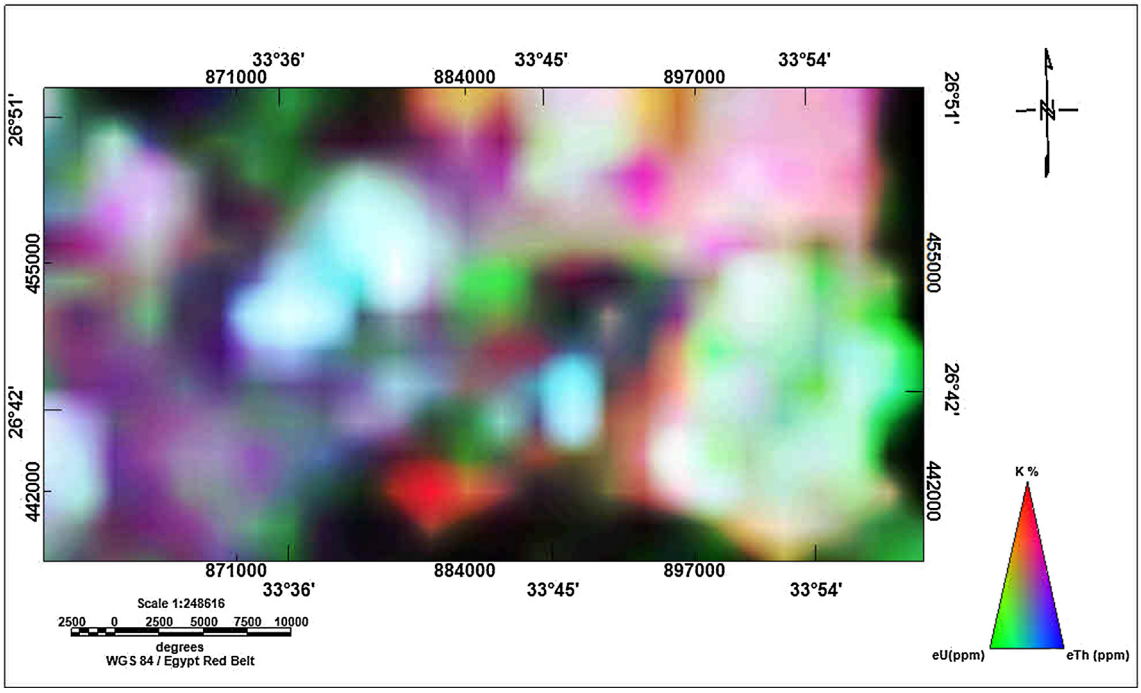

Fig. 7. False-color radioelement composite image of the study area.

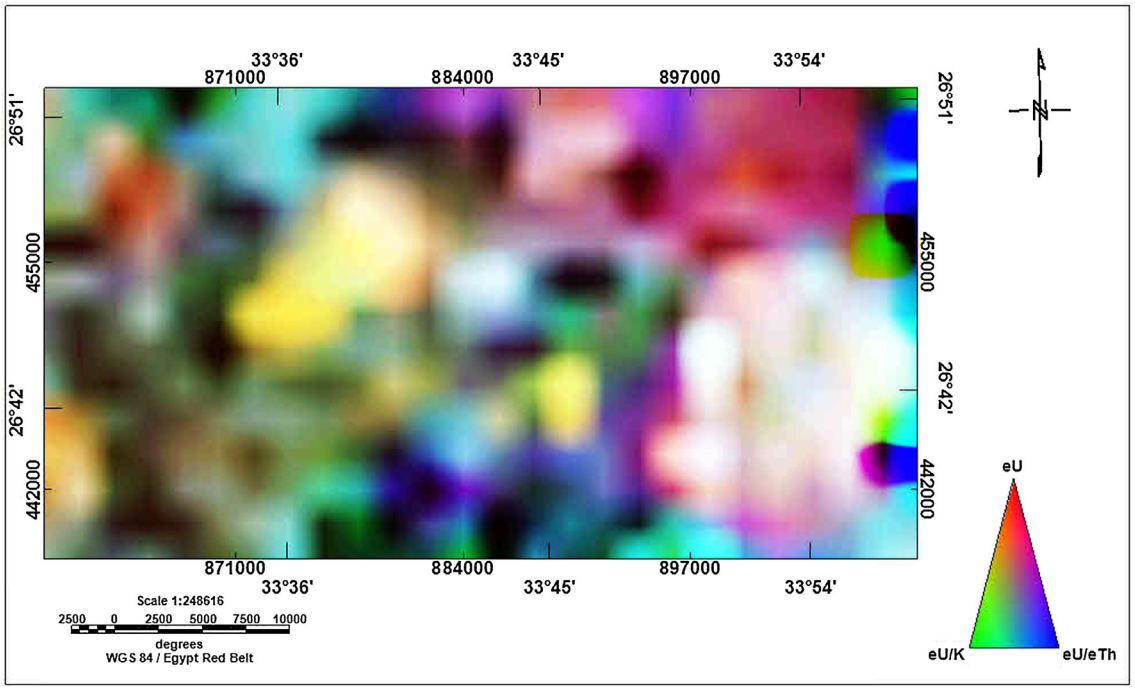

Fig. 8. False-color uranium composite image of the study area.

2.4. False-color radioelement composite image

It is denoted as a composite image of absolute radioelement K%, eU and eTh. The red, green and blue (RGB) color combination was used to produce this composite image. The integration of the geologic map and the ternary map of the area (Figs. 2 and 7) reveals a remarkable contrast between the mapped exposures of the predominant rock types in the southeastern and the northwestern parts (white color). The highly white color, which indicates an increase of the three radioelement is mainly related to the younger granites and the older granites. The moderate colors which appear as green and violet colors are associated with the Wadi deposits. The dark colors, which indicate low concentration of the three radioelements all over the mapped area, are closely related to the metagabbro rocks that clearly identified on the ternary image.

2.5. The false-color composite images for Uranium, Thorium and Potassium

The Uranium composite image (Fig. 8) provides useful information of anomalous zones of Uranium concentration. This image combines eU in red, with two ratios eU/K% (in green) and eU/e Th (in blue). As illustrated from the image, the uranium anomalous zones are displayed

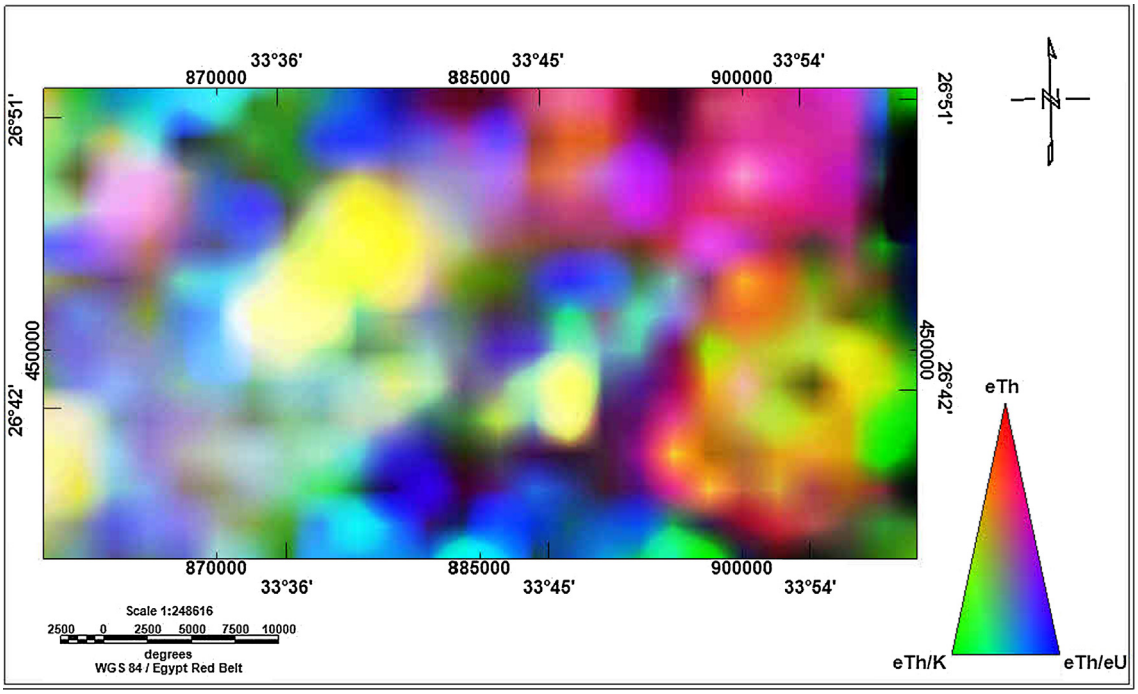

Fig. 9. False-color thorium composite image of the study area.

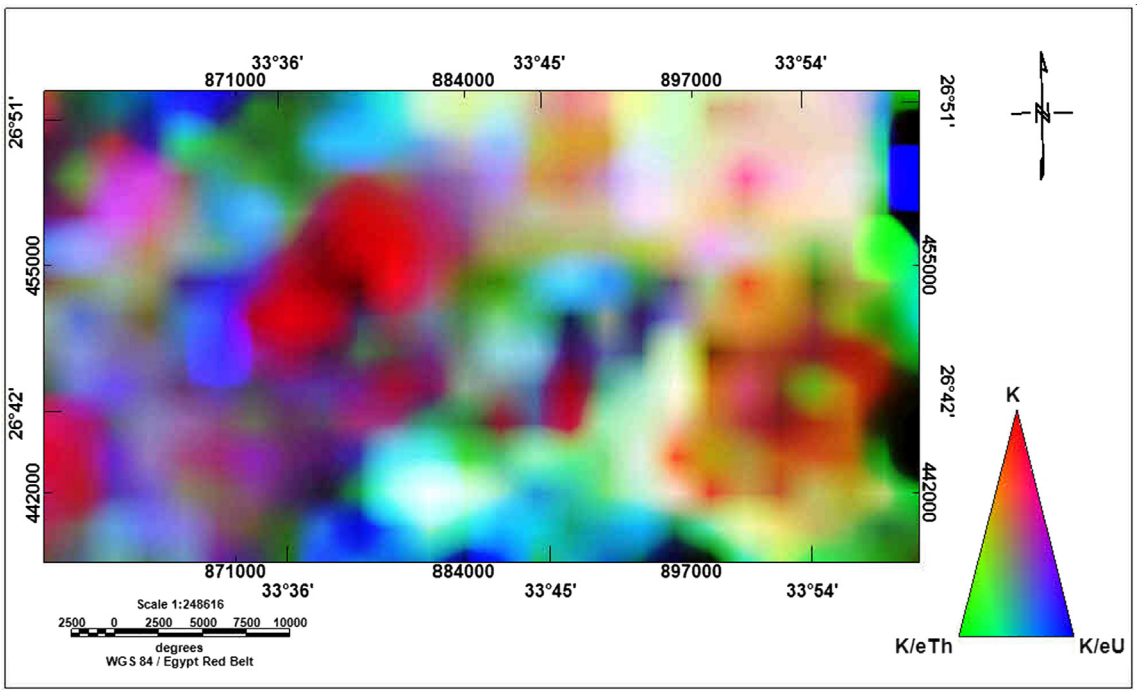

Fig. 10. False-color potassium composite image of the study area.

as bright color areas, representing in the southeastern part of the study area.

The thorium image combines eTh in red with two ratios eTh/K% (in green) and eTh/eU (in blue) (Fig. 9). This image indicates the relative distribution of thorium. The bright white color on this image is good pointer to areas where thorium has been preferentially enriched relative to both K% and eU. It is noticed that the same observed bright colors were mainly associated with some parts of the granitic rocks.

The Potassium composite image (Fig. 10) combines K% (in red) with two ratio K%/eTh (in green), and K%/eU (in blue). The image shows the Potassium concentration (the bright color) in relative to eU and eTh, which associated to the sediments and the deposits in the Wadis, which separate the hills of the granetic rocks.

2.6. Aeromagnetic data

The aeromagnetic survey is a powerful tool in delineating the regional geology (lithology and structure) of buried basement terrain. The detailed aeromagnetic map is providing illustration similar to the geology of the study area (Aero-Service, 1984). The secondary magnetic field is produced from the magnetic minerals in the crust of the earth, illustrates the distribution of these minerals. The main magnetic field,

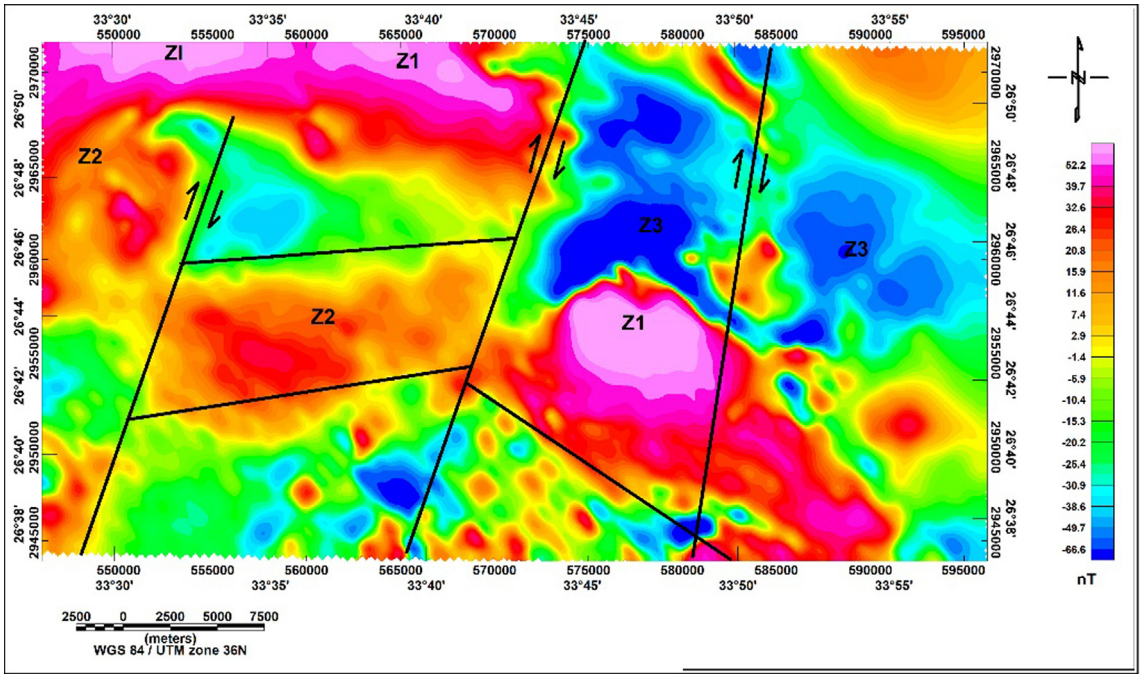

Fig. 11. Reduced to north magnetic pole(RTP) in nT, of the study area, showing the possible faults and the distinct magnetic zones.

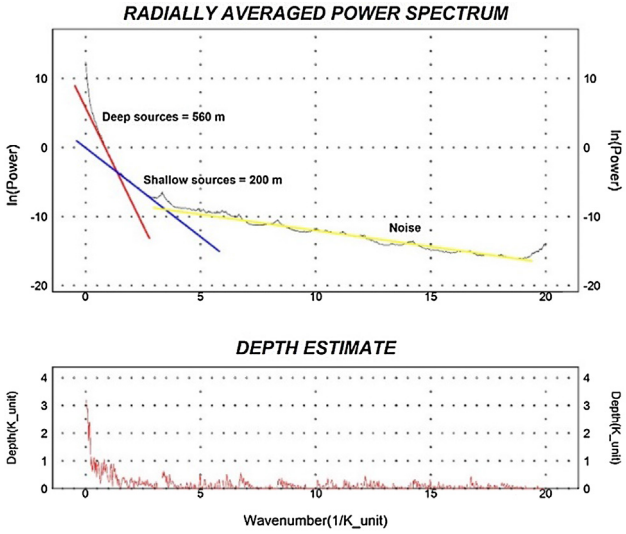

Fig. 12. Radial averaged power spectrum and depth estimate of the RTP map of the study area.

varies slowly from one place to another. However, the crustal field, is a part of the magnetic field associated with the magnetization of the crustal rocks, containing both magnetism caused by induction from the main magnetic field and from remnant magnetization, varies more rapidly. The airborne magnetometer records these variations in the total magnetic field. The regional correction of the magnetic data removes a great part of the primary field of the earth, so that the variety of the secondary field are emphasized. The interpretation of the aeromagnetic survey data illustrates directly the geological information by looking at the map without any calculations (Boyd, 1969).

2.7. Aeromagnetic data interpretation

The RTP map shows that the southeastern and the northwestern portions display high magnetic anomalies (Fig. 11). There is apparently a geochemical change in the older granite as a whole, with similar rock types mapped on either side of the boundary displaying the change. Also, the mapped younger granite at the northwestern side of the area appears to be magnetically transparent.

Technique of spectral analysis provides an averaging depth estimated from regularly-spaced digital field data as shown in (Fig. 12). The calculated average depths equal 560 m for the regional component and 200 m for the residual one. Wavelength filtering (Gaussian technique) is applied to calculate the regional and residual fields. The Gaussian technique is used to do the regional, residual separation because of its perfect separation with lowest effect from any surrounding noise. Gaussian technique also has no weaker false anomalies, even in noisy and culturally environment plus no ringing problems (Ismail, 2008). The residual and regional magnetic-component maps obtained are shown in Figs. 13 and 14 respectively.

The residual magnetic anomalies can be defined as the anomalies that are economically interesting, because they indicate local and shallow bodies and are characterized by weaker anomalies.

The RTP and the regional maps reveal several faults in the NW-SE direction (Figs. 11 and 14), these may be significant since mineralization of economic importance either radioactive and/or magnetic, might be associated with them.

The qualitative interpretation of the RTP, the residual (near-surface) and the regional (deep-seated) components maps, reveals clear positive anomalies over the basement rocks (the older granite and the younger granite). The positive magnetic anomaly is circular in the plane view and centered on the mapped outline of the older granite.

The RTP and regional magnetic maps show clearly three distinct magnetic zones. The first zone(Z1) is characterized by high magnetic amplitude in the northwestern and the southeastern parts of the study area. As shown from the geologic map (Fig. 2), this zone is associated with the older granite and younger granite rocks. The second zone(Z2) is encountered in the northwestern side of the study area. It is characterized by low magnetic amplitude with oval shape. This zone is associated with the younger granites. The third zone(Z3) occurs at the northeastern part of the area. It is characterized by relatively very low magnetic amplitude.

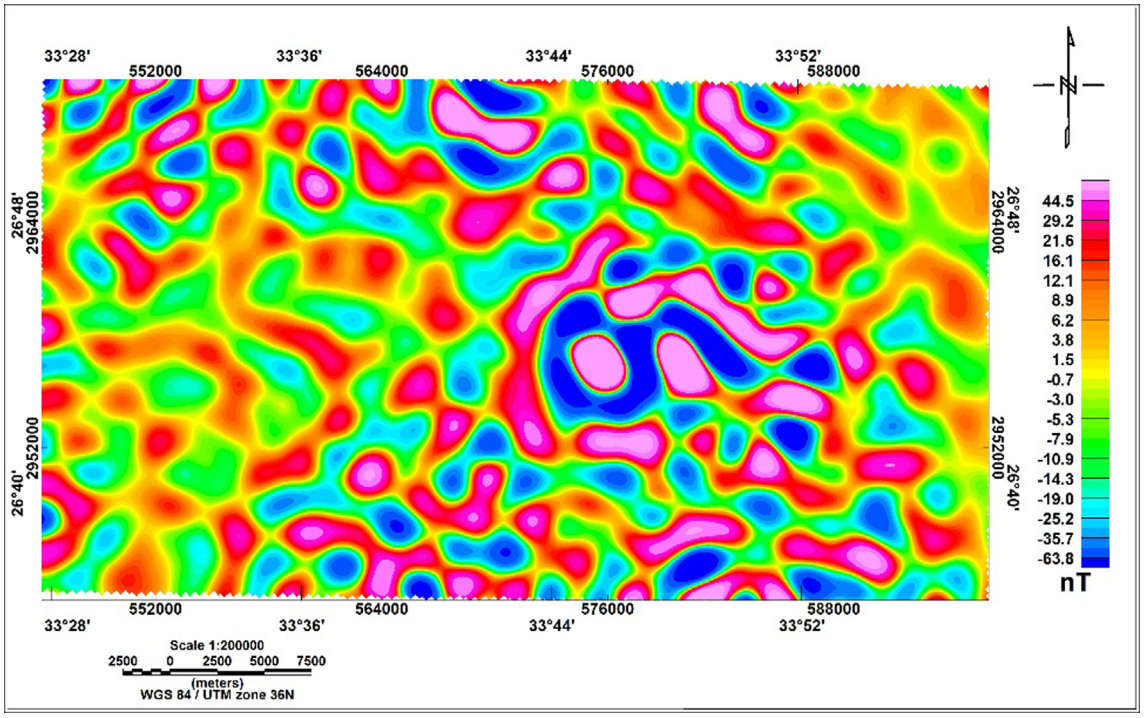

Fig. 13. Resiual (high-pass) magnetic map of the study area.

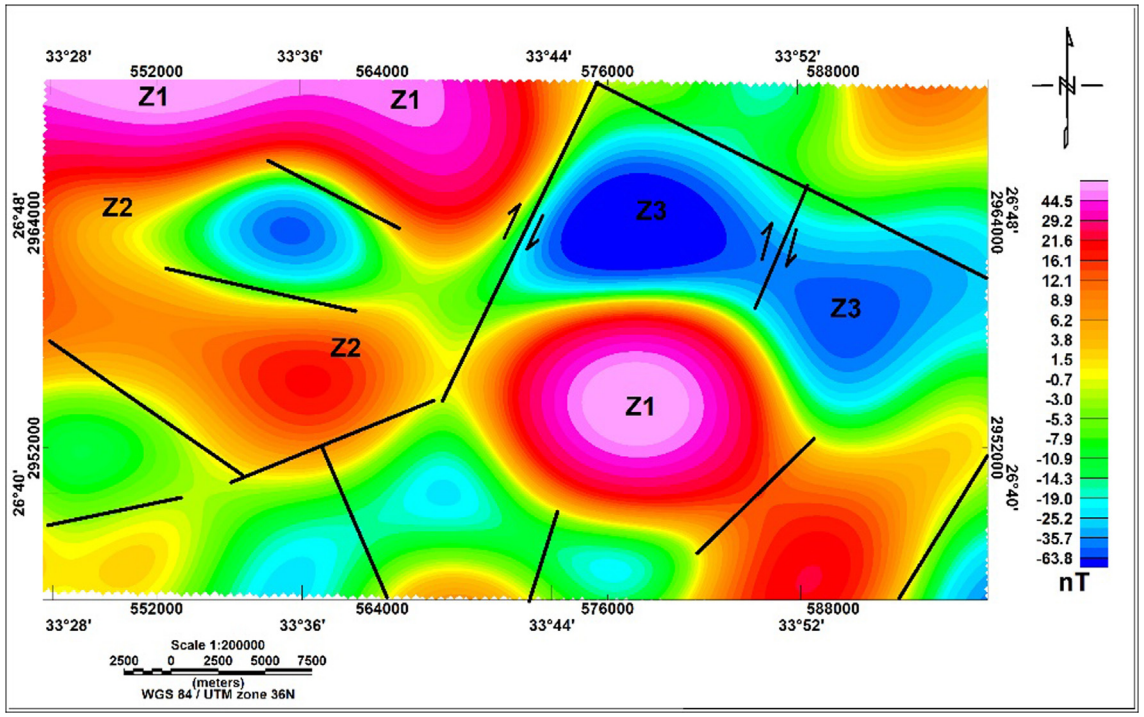

Fig. 14. Regional (low-pass) magnetic map of the study area showing the possible faults and the distinct magnetic zones.

2.8. The satellite imagery data

Multispectral remote-sensing has been used for lithological and mineral mapping especially with the applying of the remote sensing sensors and mathematical algorithms that provided detailed information of the mineralogy of the various rock types comprising the Earth's surface (Zhang et al., 2007).

Different satellite sensors, such as; Landsat-5 (TM), landsat-7 (ETM +) and (ASTER) imagery have been achieved for extraction the spectral information related to the type of the study (Vincent, 1997). Since the ASTER channels are more contiguous in the short wave infrared region than those of the Landsat, this made the ASTER data better than the other satellite data for the lithological mapping (Crosta et al., 2003). Two kinds of satellite images have been used in the current study, Landsat TM and Aster images.

For the Landsat-5 (TM) images, false color composite image was made in RGB colors of bands 2, 4 and 7 and also band ratio image was made in RGB colors of band ratio (5/7, 5/4 and 5/1) to clear the rock

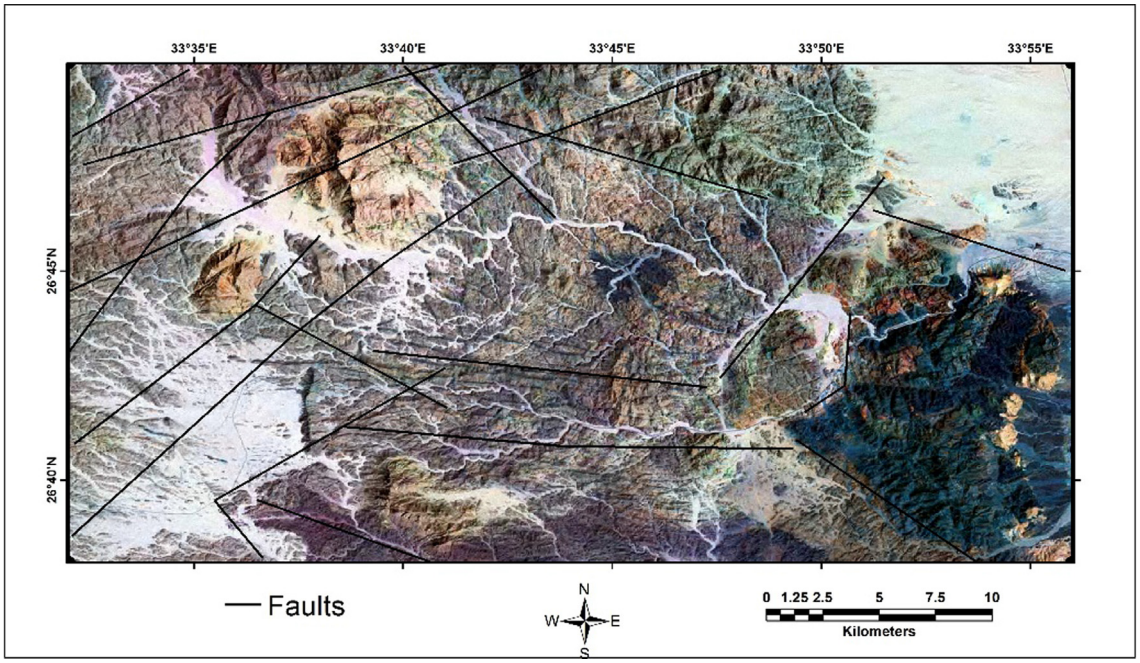

Fig. 15. TM landsat false composite color image in RGB (2, 4 and 7 bands) of the study area.

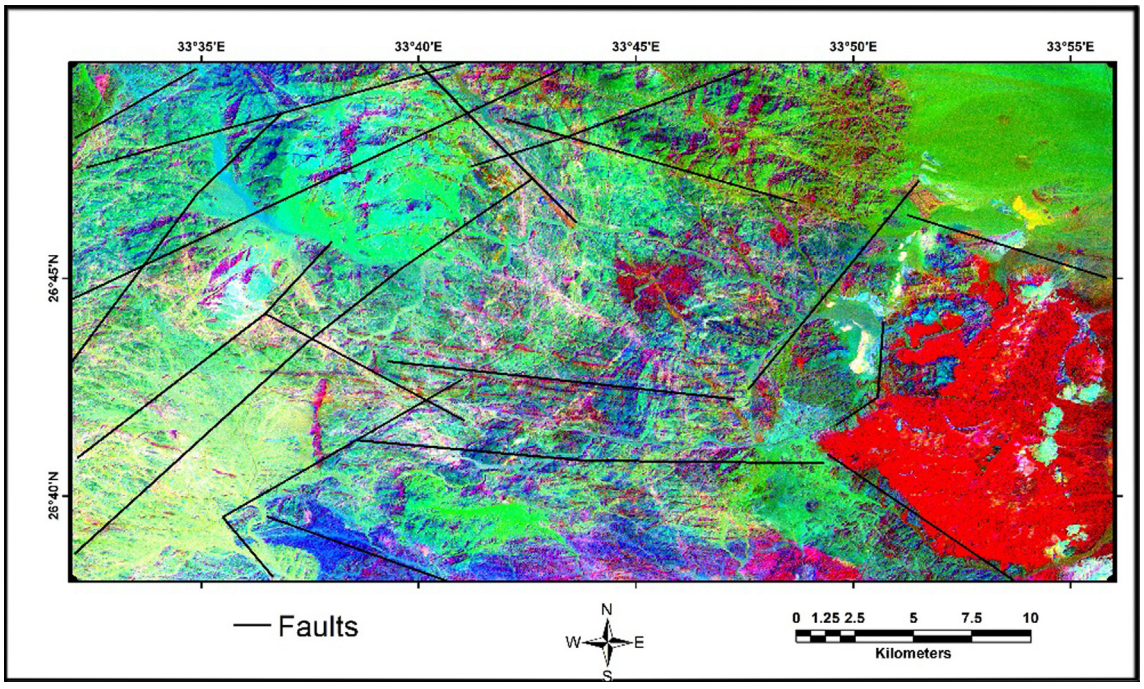

Fig. 16. TM landsat false composite color image of bands ratio in RGB (5/7.5/1 and 5/4) of the study area.

boundaries. From the interpretation of false color composite images of TM bands 2, 4 & 7 and band ratio image (Figs. 15 and 16) in RGB, it can discriminate the boundary of rock units depending to the color differences and photo geological characteristics of rocks. The Quaternary deposits of the wadi sediments have light white color, Dohan volcanics have dark blue color, the older granites have dark brown and the younger granites have light brown color. From the band ratio image, the rock units show different colors, Dohan volcanics have red color, The Quaternary deposits of the wadi sediments have green color, the older granites have light blue, and the younger granite have light green color. From the rock boundaries, it can deduce and detect the surface structures which separate and cut the rock unites, which are mainly appeared in the northwestern and the southeastern parts of the study area (Fig. 17).

From the Aster images, the obtain seen cover the most parts of the study area, the boundaries of the rock units appear more clearly because of the high resolution of the ASTER seen. False composite color image was made of bands (7, 3 and 1) in RBG color image. Dokhan volcanic rocks have a dark pink, the older granite has light pink, the younger granite has light green, the Quaternary deposits of the wadi sediments have light white color. The surface faults and the fractures can be easy detected from the high resolution of the rock boundaries (Fig. 18). The another processing which has been made, is the band ratio image in RGB false composite color (4/7, 4/3 & 4/), this image

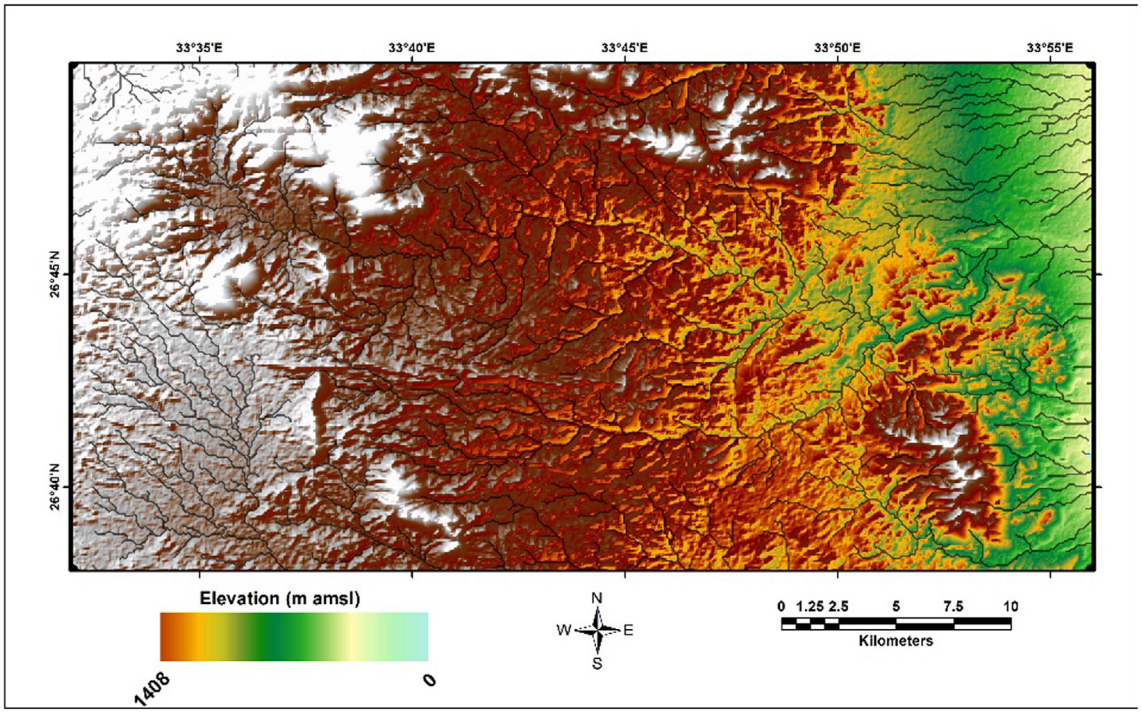

Fig. 17. The DEM map of the study area.

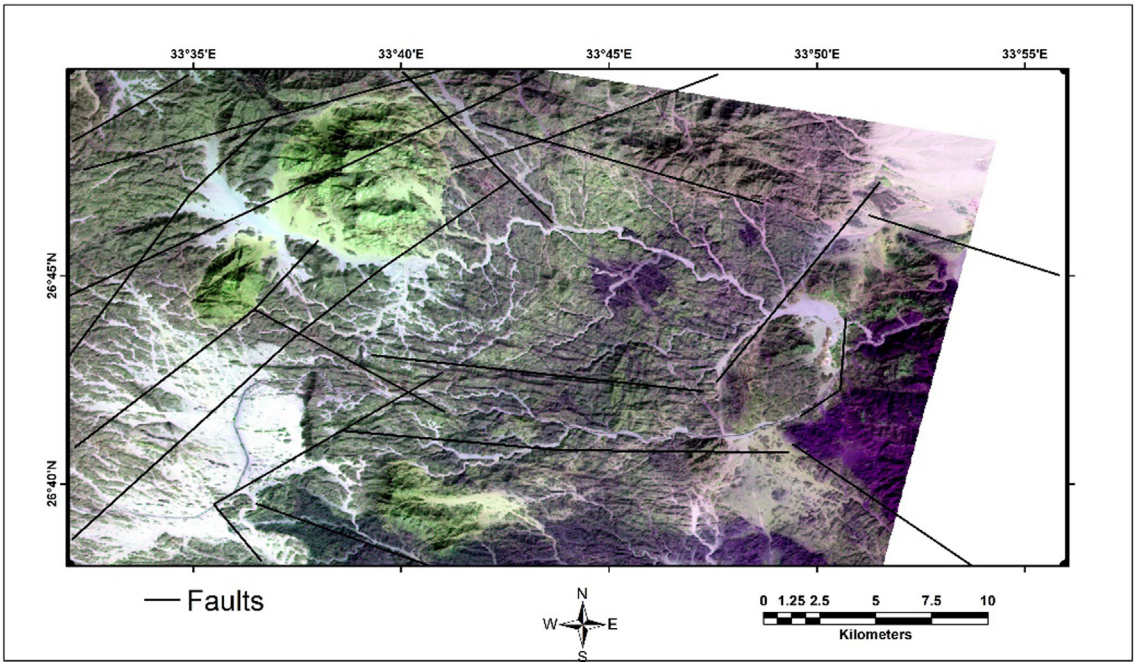

Fig. 18. Aster false composite color image in RBG (7, 3 and 1 bands) of the study area.

(Fig. 19) shows the Dokhan volcanic rocks with dark red color, the older granite with light red color, the younger granite with light green, the Quaternary deposits of the Wadi sediments with light brown and light pink respectively. The high resolution band ratio image clearly shows the places of the available faults and the fractures, and this is the main target of applying the satellites images in the current study.

The satellite images (Landsat-5(TM) and ASTER images) after processing show several surface faults and fractures in the northeastern and the southwestern parts of the study area according to the rock color variations in RGB color, textural variations, rock units displacement and from the drainage patterns.

2.9. Data results integration

According to the visual interpretation of the regional magnetic map, radioelement composite image, Landsat TM band ratio and Aster band ratio maps, it is found that, the radioelement composite image shows the radioactive zones over the rock units in the study area (Fig. 20A), the regional magnetic map reveals the location of the major tectonic structures (Fig. 20B), and the satellites images of Landsat TM and Aster band ratio both revealing the surface faults and fractures in the study area (Fig. 20C and D). The location of all of these fractures are in the northwestern and the southeastern parts of the study area. From these

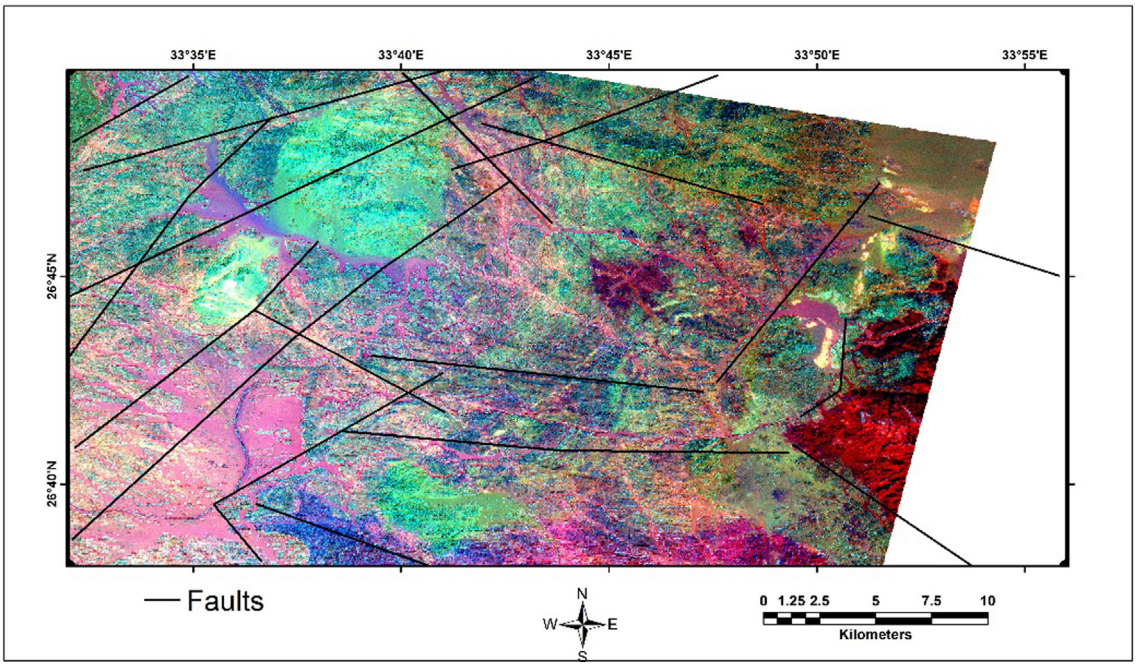

Fig. 19. Aster false composite color image of band ratio (4/7, 4/1 and 4/3) in RBG of the study area.

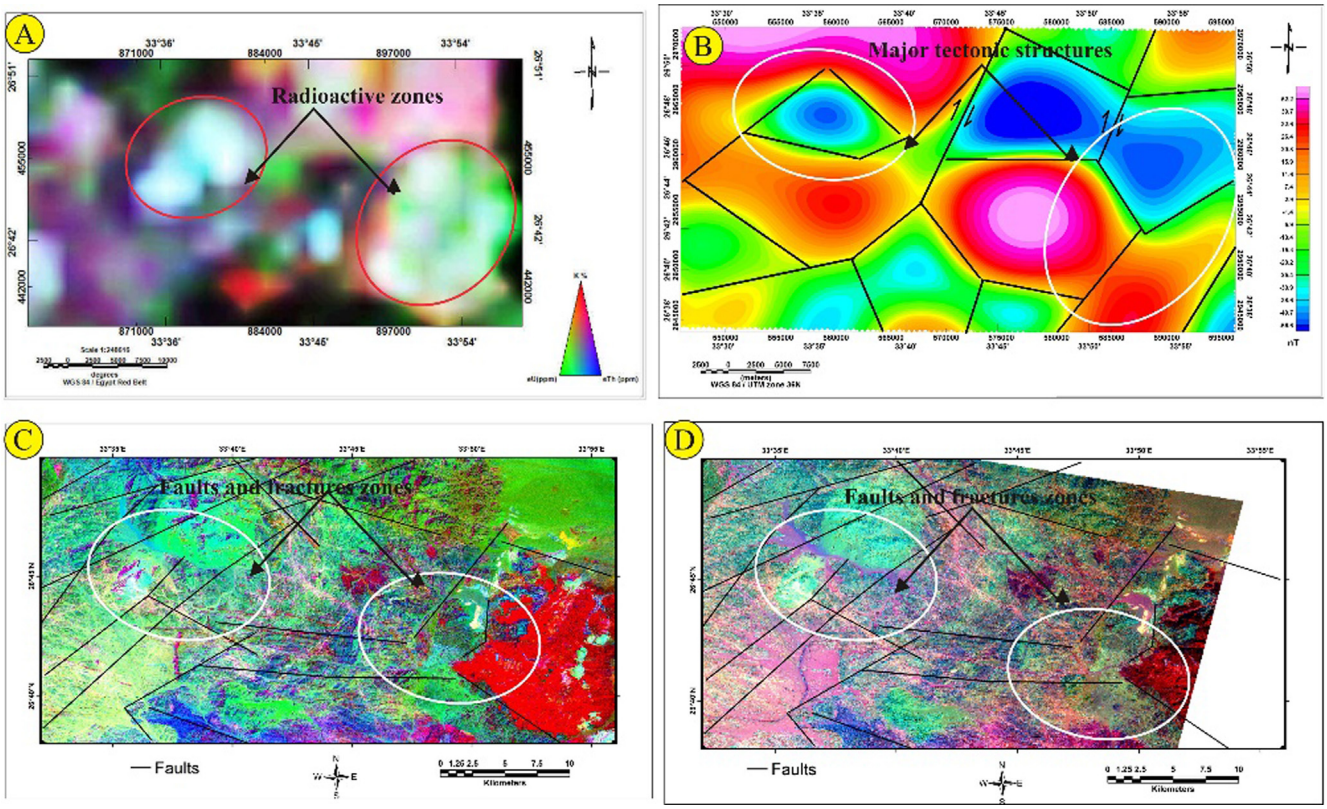

Fig. 20. Integration of data results of the study area; (A) radioelement composite image, (B) Regional (low-pass) magnetic map, (C) TM landsat composite image of bands ratio and (D) Aster composite image of band ratio.

results, it is clear that there is a relative correlation between the radioactive zones as shown from the radiometric maps, the location of the faults and the fractures that have been shown from the magnetic maps and the satellite images, which have affected the presence of the radioactive mineralization zones, and this is the target from the current study, which is to determine the location of the radioactive anomolous zones associated with the occurrence of the geological structures.

3. Conclusions

The study area is mainly occupied with Precambrian basement rocks that comprise older granitoids, younger granites and Dokhan volcanics which injected by basic and acidic dykes of different attitudes. The exposure rock units are traversed by many valleys filled with alluvial deposits of Quaternary age.

From the obtained results of the three used data (airborne gamma-ray spectrometric, airborne magnetic and the satellite imagery) it can conclude the following:

The highest radioactive zone is associated with the granitic rocks. This zone which is distributed in all maps is related to the presence of younger granites, older granites, and the microgranit dykes that are cutting the Dokhan Volcanic.

The RTP and regional magnetic maps show clearly three distinct zones. The first zone is characterized by high magnetic amplitude in the northeastern and the southwestern parts of the study area. As shown from the geologic map, this zone is associated with the older granite and younger granite rocks. The second zone is encountered in the Northwestern side of the study area. It is characterized by low magnetic amplitude with oval shape. This zone represents the younger granites rocks. The third zone represents the northeastern side of the area and is characterized by very low magnetic amplitude. The separated zones between the high and low magnetic amplitude is the possible places for the faults and the fractures between the different types of the rocks in the study area, this is almost correlated by the high radioactive zones. The residual magnetic anomalies can be defined as the anomalies that are economically interesting, because they indicate local and shallow bodies and are characterized by weaker and more localized anomalies. The RTP and the regional maps show several faults trending in the NW-SE direction, which may be significant since mineralization of economic importance either radioactive and/or magnetic, might be associated with them.

The processed satellite images of TM landsat and ASTER images observe the possible places of the surface faults and the fractures in the studied area over the rock types which are approximately correlated to the obtained results from the radioactive and the magnetic maps, and this is the main target of the current study area.

The integration of the radiometric, magnetic and satellite images aided by geological information helps to detect the anomalous radioactive zones in the area of study.

However, the recommendation after these results is doing ground geophysical surveying in southeastern and northwestern parts of the study area over the basement rocks and the areas surrounded the granitic dykes to confirm the presence of the economic radioactive mineralization zones.

References

Aero-Service, 1984. Final operational report of airborne magnetic-radiation survey in the Eastern Desert, Egypt, for the Egyptian General Petroleum Corporation. Aero-Service Division, Houston, Texas, April 1984, six volumes.

Boyd, D., 1969. The contribution of airborne magnetic surveys to geological mapping. In "Mining and Ground Water Geophysics", Geol. Surv. Of Canada, Economic Geology Report No. 26, pp. 213–227.

Conco Coral Corporation and the Egyptian General Petroleum Corporation(EGPC), 1987. Geological map of Egypt, Scale 1:500000-NG 36 SE-QUSEIR.

Crosta, A.P., Souza Filho, C.R., Azevedo, F., Brodie, C., 2003. Targeting key alteration minerals in epithermal deposits in Patagonia, Argentina, using ASTER imagery and principal component analysis. Int. J. Rem. Sens. 23, 4233–4240.

EL Hadary, A., El Azab, A., Omran, A.A., 2013. Contributions to the geology and mineralogy of wadi Ras Abda area, North Eastern Desert, Egypt. Nucl. Sci. Sci. J. 2.

Geosoft package, 2002. Geosoft Mapping and Processing System, Geosoft Inc., Toronto.

International Atomic Energy Agency (IAEA), 2003. Guidelines for Radioelement Mapping Using Gamma-ray Spectrometric Data, Technical Reports SeriesNo., IAEA-TECDOC-1363, Vienna, p. 179.

Ismail, A.A.M., 2008. A Study of the Effects of Various Regional-Residual.

Raslan, M.F., Ali, M.A., 2011. Mineralogy and mineral chemistry of rare-metal pegmatites at Abu Rusheid granitic gneisses, South Eastern Desert, Egypt. Geologija 54 (2), 205–222. https://doi.org/10.5474/geologija.2011.016.

Rogers, J.J.W., Adams, J.S.S., 1969. Uranium. In: Wedepohl, K.H. (Ed.), Handbook of Geochemistry. Springer-Verlag, New York 92 B1–92 C10.

Schürmann, H.M.E., 1966. The precambrian of the Gulf of Suez and the northern part of the Red Sea. E.J. Brill, Leiden. Netherland, 404 p.

Vincent, R.K., 1997. Fundamentals of Geological and Environmental Remote Sensing: Upper Saddle River. Prentice-Hall, NJ.

Zhang, X., Pazner, M., Duke, N., 2007. Lithologic and mineral information extraction for gold exploration using ASTER data in the south Chocolate Mountains (California). Photogram. Rem. Sens. 62, 271–282.